Eighth Australasian Fluid Mechanics
Conference, University of Newcastle,
N.S.W., 28 November/2 December 1983.

BUBBLE GROWTH BY MARKER AND CELL TECHNIQUE

H.D. ZUGHBI, W.V. PINCZEWSKI & C.J. FELL

SCHOOL OF CHEMICAL ENGINEERING & INDUSTRIAL CHEMISTRY

UNIVERSITY OF NEW SOUTH WALES, KENSINGTON, NSW. 2033 AUSTRALIA

SUMMARY A numerical model is developed to describe the bubbling process at a submerged orifice. The model is based on a modified Marker and Cell (MAC) technique and rigorously accounts for the effect on bubble growth of boundaries confining the liquid flow field. Good agreement is demonstrated between the model predictions and experimentally observed bubble shapes and growth rates. The model is applicable to both 'deep-pool' and 'shallow pool' bubbling regimes and clearly shows the development of a high velocity wall jet along the tray floor which detaches the growing bubble from the orifice.

1 INTRODUCTION

The bubbling of a gas through a liquid is the basis for many important industrial gas-liquid contacting processes. Distillation and absorption tray contactors, pyrometallurgical reactors, and hydrogenation of liquids derived from coal liquidation and oil shale retorting are but a few examples. In this process the bubbles are formed by the injection of a gas through a submerged orifice and a number of theoretical models have been developed to describe the complex interaction which takes palce between the liquid and injected gas during bubble formation. The earlier models (Davidson and Schuler (1960), McCann and Prince (1969), Kupferberg and Jameson (1969)) were all based on the assumption of spherical growth and required the specification of an arbitrary detachment criteria to terminate the growth of the bubble. More recently Marmur and Rubin (1976) and Pinczewski (1981) have shown that bubble detachment occurs as a natural consequence of the dynamics of the bubbling system.

Although all of the above models have been demonstrated to be in reasonable agreement with a range of experimental observations, the agreement is limited to conditions of 'deep-pool' bubbling. This is because all the models are based on the simplifying assumption that the bubble grows in a liquid of infinite extent. Under conditions of 'shallow-pool' or imperfect bubbling where the orifice is shallowly submerged and where the limited extent of the liquid has a significant effect on bubbling behaviour (McCann and Prince (1971)) the models are clearly inappropriate.

The purpose of the present paper is to describe a general model for bubble growth at a submerged orifice which is capable of describing the phenomena of non-spherical bubble growth and which can account for the effects of boundaries which limit the extent of the liquid above the orifice. Such a model would be applicable to all the regimes of bubbling at a submerged orifice. The model described is based on a modified Marker and Cell (MAC) method (Harlow and Welch (1965), Chan and Street (1970)) in which the unsteady, incompressible, axisymmetric Navier-Stokes equations describing the liquid flow field about the growing bubble are solved in the primitive variables of velocity and pressure using a staggered finite difference technique.

2. FORMULATION OF BUBBLE GROWTH PROBLEM

A schematic of the bubbling problem is shown in Figure (1). The orifice of radius R_h is located in the centre of a plate which separates a gas chamber of volume V_c and a liquid of depth H which is bounded by the plate and the cylindrical wall of the containing vessel.

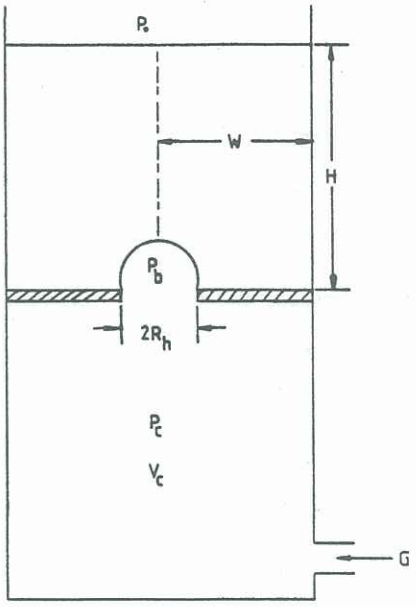

Figure 1 - Schematic of Bubble Growth Problem

Gas is introduced into the chamber at a constant volumetric rate G.

Assuming that the bubble is axisymmetric and that the liquid is incompressible, the motion of the liquid bounded by the growing bubble surface, the plate floor, the container wall and the air-liquid interface is governed by the Navier-Stokes equations:

$$\frac{\partial u}{\partial t} + u\frac{\partial u}{\partial x} + v\frac{\partial u}{\partial y} = -\frac{\partial \phi}{\partial x} + g_x + \nu\left[\frac{\partial^2 u}{\partial x^2} + \frac{\partial^2 u}{\partial y^2} + \varepsilon\left(\frac{1}{x}\frac{\partial u}{\partial x} - \frac{u}{x^2}\right)\right] \quad (1)$$

$$\frac{\partial v}{\partial t} + u\frac{\partial v}{\partial x} + v\frac{\partial v}{\partial y} = -\frac{\partial \phi}{\partial y} + g_y + \nu\left[\frac{\partial^2 v}{\partial x^2} + \frac{\partial^2 v}{\partial y^2} + \varepsilon\left(\frac{1}{x}\frac{\partial v}{\partial x}\right)\right] \quad (2)$$

Where (u,v) are the velocity components in the cylindrical coordinate directions (r,z) when $\varepsilon = 1$ and the Cartesian coordinate directions (x,y) where $\varepsilon = 0$. ϕ is the ratio of pressure to constant density (P/ρ_l). ν is the kinematic viscosity coefficient when the flow is laminar and an effective or eddy viscosity

(Gorman (1969)) which accounts for the effect of turbulence on the transport of momentum when the flow in the liquid is turbulent. g_x and g_y are the body (gravity) accelerations.

The continuity equation is written as:

$$\frac{\partial u}{\partial x} + \frac{\partial v}{\partial y} + \varepsilon\frac{u}{x} = D = 0 \qquad (3)$$

Where D is the divergence.

Operating with $\frac{\partial}{\partial x}$ on equation (1) and $\frac{\partial}{\partial y}$ on equation (2) and then adding the results we have:

$$\frac{\partial^2 \phi}{\partial x^2} + \frac{\partial^2 \phi}{\partial y^2} = -R \qquad (4)$$

where

$$R = \tfrac{1}{2}\frac{\partial^2 u^2}{\partial x^2} + \tfrac{1}{2}\frac{\partial^2 u^2}{\partial y^2} + \frac{\partial^2 (uv)}{\partial x \partial y} + \frac{\partial D}{\partial t}$$

$$- \nu\left[\frac{\partial^2 D}{\partial x^2} + \frac{\partial^2 D}{\partial y^2} + \varepsilon\left(\frac{-D}{x^2} + \frac{1}{x}\frac{\partial D}{\partial x} - \frac{\partial}{\partial x}\left(\frac{u}{x^2}\right)\right)\right]$$

Equations (1) to (4) are the basic MAC equations which, with the appropriate boundary conditions, may be solved for the pressure and velocity fields in the liquid. The velocities may then be used to move massless marker particles which define the position of the bubble surface to obtain the evolution of the bubble surface with time.

2.1 Boundary Conditions

(a) Solid Walls

Since the vessel walls and plate floor containing the liquid are impermeable the velocity component normal to the walls must be zero i.e. $q_N = 0$. For the velocity condition tangential to the wall, the wall may be treated as either a 'free-slip' or 'no-slip' boundary. In practice, the effect of the boundary layer at the wall is usually small and this suggests the use of a free-slip condition. Moreover, when treating turbulent flows a non-slip condition at the wall would result in the generation of artificially large boundary layers under conditions when the eddy diffusivity is large. We therefore use the condition $\frac{\partial q_T}{\partial n} = 0$ throughout.

(b) Air-liquid Interface

In experimental studies it is usual to maintain the height of liquid level above the tray constant by the provision of an overflow wier. In the computations we have therefore fixed the position of the air-liquid interface in space and time and prescribed a constant applied pressure, P_o, which is usually atmospheric.

(c) Bubble Surface

The liquid phase pressure, P, at any point on the bubble surface is related to the pressure within the bubble, P_b, by,

$$P = P_b - \frac{2\sigma}{R} \qquad (5)$$

where σ is the surface tension and R is the local radius of curvature of the bubble surface. Limiting the present treatment to cases where it is possible to neglect the effect of gas momentum i.e. $\rho_g \cong 0$, the pressure within the bubble is everywhere uniform.

The bubble pressure, P_b, is related to the chamber pressure, P_c, by the usual orifice equation

$$P_c - P_b = \rho_g K V_h^2 \qquad (6)$$

where K is the orifice coefficient and V_h is the average velocity of gas through the orifice.

Assuming that the conditions within the bubble are isothermal, incompressible (ρ_g = constant) and that internal specific energy remains approximately constant, the flow rate through the orifice is related to the rate of bubble growth by

$$V_h = \frac{1}{A_h}\left(\frac{dV_b}{dt}\right) \qquad (7)$$

where A_h is the area of the orifice and V_b is the bubble volume which is a function of time.

Further assuming adiabatic behaviour in the gas chamber, V_c, the chamber pressure, P_c, (Kupferberg and Jameson (1969)) is given by:

$$P_c = P_{c|t=0} - \frac{C_o \rho_g}{V_c}\left[(V_{b|t} - V_{b|t=0}) - Gt\right] \qquad (8)$$

where C_o is the sonic velocity in the gas of density ρ_g.

Equations (5) to (8) relate the pressure on the liquid side of the bubble interface to the rate of gas injection into the gas chamber G.

3 COMPUTATIONAL PROCEDURE

The liquid region is divided into a number of rectangular cells (i,j) of size Δx and Δy as shown in Figure (2). Velocities are defined at cell boundaries and pressures at cell centres. If velocities are required at other locations they are obtained by simple interpolation. In the present work it was found that the interpolation was best carried out along lines normal to the bubble surface. The Navier-Stokes equations (1) and (2) are differenced using an explicit central difference form for all the spatial derivatives except pressure. The results are:

$$u^{n+1}_{i+\frac{1}{2},j} = u^n_{i+\frac{1}{2},j} + \Delta t\left[\frac{(u^n_{i,j})^2 - (u^n_{i+1,j})^2}{\Delta x} + g_x\right.$$

$$+ \frac{(uv)^n_{i+\frac{1}{2},j-\frac{1}{2}} - (uv)^n_{i+\frac{1}{2},j+\frac{1}{2}}}{\Delta y} + \frac{\phi^{n+1}_{i,j} - \phi^{n+1}_{i+1,j}}{\Delta x}$$

$$+ \nu\left(\frac{u^n_{i+3/2,j} + u^n_{i-\frac{1}{2},j} - 2u^n_{i+\frac{1}{2},j}}{\Delta x^2}\right.$$

$$\left.+ \frac{u^n_{i+\frac{1}{2},j+1} + u^n_{i+\frac{1}{2},j-1} - 2u^n_{i+\frac{1}{2},j}}{\Delta y^2}\right.$$

$$\left.\left.+\varepsilon\left(\frac{1}{x_{i+\frac{1}{2},j}}\left(\frac{u^n_{i+1,j} - u^n_{i,j}}{\Delta x} - \frac{u^n_{i+\frac{1}{2},j}}{(x_{i+\frac{1}{2},j})^2}\right)\right)\right)\right] \qquad (9)$$

$$v^{n+1}_{i,j+\frac{1}{2}} = v^n_{i,j+\frac{1}{2}} + \Delta t\left[\frac{(v^n_{i,j})^2 - (v^n_{i,j+1})^2}{\Delta y}\right.$$

$$+ \frac{(uv)^n_{i-\frac{1}{2},j+\frac{1}{2}} - (uv)^n_{i+\frac{1}{2},j+\frac{1}{2}}}{\Delta x} + g_y$$

$$+ \frac{\phi^{n+1}_{i,j} - \phi^{n+1}_{i,j+1}}{\Delta y}$$

$$+ \nu\left(\frac{v^n_{i,j+3/2} - 2v^n_{i,j+\frac{1}{2}} + v^n_{i,j-\frac{1}{2}}}{\Delta y^2}\right.$$

$$\left.+ \frac{v^n_{i+1,j+\frac{1}{2}} - 2v^n_{i,j+\frac{1}{2}} + v^n_{i-1,\,j+\frac{1}{2}}}{\Delta x^2}\right.$$

$$+ \varepsilon \left(\frac{1}{\bar{x}_{i,j+\frac{1}{2}}} \left(\frac{v^n_{i+\frac{1}{2}j,j+\frac{1}{2}} - v^n_{i-\frac{1}{2},j+\frac{1}{2}}}{\Delta x}\right)\right)\Big] \qquad (10)$$

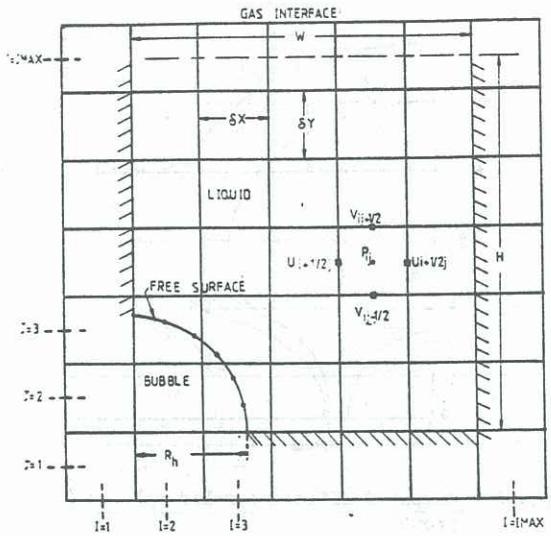

Figure 2 - MAC discretization of liquid flow field

Equations (9) and (10) allow velocities at time level (n+1) to be calculated explicitly provided that ϕ^{n+1} values are available. These are obtained from a prior solution of the pressure equation (4) using an iterative (point successive over-relaxation) procedure based on the finite difference analogue of equation (4):

$$\phi^{n+1,k+1}_{i,j} = \frac{\eta_1\eta_2\eta_3\eta_4}{2(\eta_2\eta_4+\eta_1\eta_3)} \left[\frac{\eta_3\phi^{n+1,k}_{i+1,j} + \eta_1\phi^{n+1,k}_{i-1,j}}{\frac{\eta_1\eta_3}{2}(\eta_1+\eta_3)}\right.$$

$$\left. + \frac{\eta_4\phi^{n+1,k}_{i,j+1} + \eta_2\phi^{n+1,k}_{i,j-1}}{\frac{\eta_2\eta_4}{2}(\eta_2+\eta_4)} + R_{i,j}\right] \cdots \qquad (11)$$

Where the coefficients $\eta_1\eta_2\eta_3$ and η_4, are defined in Figure 3 and $R_{i,j}$ is given by

$$R_{i,j} = \frac{(u^n_{i+1,j})^2 - 2(u^n_{i,j})^2 + (u^n_{i-1,j})^2}{(\Delta x)^2}$$

$$+ \frac{(v^n_{i,j+1})^2 - 2(v^n_{i,j})^2 + (v^n_{i,j-1})^2}{(\Delta y)^2}$$

$$+ \frac{2}{\Delta x \Delta y}\left[(uv)^n_{i+\frac{1}{2},j+\frac{1}{2}} + (uv)^n_{i-\frac{1}{2},j-\frac{1}{2}} - (uv)^n_{i-\frac{1}{2},j+\frac{1}{2}}\right.$$

$$\left. - (uv)_{i+\frac{1}{2},j-\frac{1}{2}}\right] - \frac{D^n_{i,j}}{\Delta t} - \nu\left[\frac{D^n_{i+1,j} - 2D^n_{i,j} + D^n_{i-1,j}}{(\Delta x)^2}\right.$$

$$\left. + \frac{D^n_{i,j+1} - 2D^n_{i,j} + D^n_{i,j-1}}{(\Delta y)^2}\right.$$

$$\left. + \varepsilon\left(\frac{-D^n_{i,j}}{(x_{i,j})^2} + \frac{D^n_{i+1,j} - D^n_{i,j}}{x_{i,j}\Delta x} - \frac{(\frac{u}{x^2})_{i+\frac{1}{2},j} - (\frac{u}{x^2})_{i-\frac{1}{2},j}}{\Delta x}\right)\right]$$

and

$$D^n_{i,j} = \frac{u^n_{i+\frac{1}{2},j} - u_{i-\frac{1}{2},j}}{\Delta x} + \frac{v^n_{i,j+\frac{1}{2}} - v_{i,j-\frac{1}{2}}}{\Delta y} + \left(\frac{u}{x}\right)^n_{i,j}$$

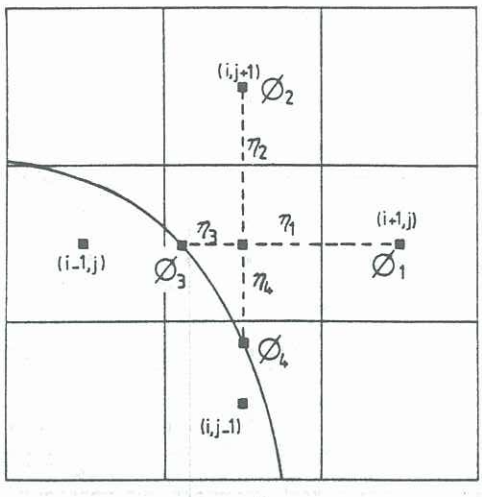

Figure 3 - Finite difference scheme for pressure solution (equation (11)).

In obtaining equation (11) from equation (4) $D^{n+1}_{i,j}$ is set to equal to zero. This is the unique feature of the MAC scheme which acts to limit the accumulation of errors resulting from the finite-difference approximations as well as computer round-off.

The initial bubble shape is assumed to be part of a shpere of radius equal to that of the orifice (Pinczewski (1981)). The initial bubble pressure is assumed to be the sum of liquid hydrostatic pressure and surface tension:

$$P_b\big|_{t=0} = P_o + \rho_1 gH + \frac{2\sigma}{R_h} \qquad (12)$$

Initial liquid velocities are assumed to be zero i.e. the liquid is initially stationary.

The numerical solution is advanced through a timestep of size Δt by using equations (5)-(7) to calculate the liquid pressure at the bubble surface. This together with the specification of boundary conditions on the solid walls and air-liquid surface allows equation (11) to be solved for the pressure field in the liquid at time level (n+1) i.e. ϕ^{n+1}. Equations (9) and (10) are then used to calculate an updated velocity field u^{n+1} and v^{n+1}.

Tracking the position of the Bubble Surface

Massless marker particles which move with the local velocity of the liquid are distributed along the bubble surface (see Figure (2)). A particle density of 2-3 per cell is usually sufficient to resolve the positioning of the bubble surface. Velocities of the marker particles u_m and v_m are interpolated from the liquid velocities previously calculated. Velocities at cells adjacent to the marker particles are used for this purpose. The new locations of the marker particles are calculated from:

$$x^{n+1}_m = x^n_m + \Delta t u_m$$

$$y^{n+1}_m = y^n_m + \Delta t v_m$$

The new marker particle positions define the new location of the bubble surface. Repetition of the above procedures results in a bubble surface which evolves with time.

4 COMPUTATIONAL RESULTS

To test the validity of the numerical model we compare our computations with experimental results reported by Kupferberg and Jameson (1969) for the air-water bubbling system. The conditions for the experiment are: R_h = 0.16cm, V_c = 2250cm^3, G = 16.7cm^3 per second and W = 6cm.

The comparison between the model and experiment is shown in Figures (4) and (5) which show results for bubble shape and bubble growth rate as a function of time. The computed results are in good agreement with the experimental measurements. Figure (4) shows that the growing bubble becomes detached from the orifice by a wall jet which establishes along the tray floor late in the bubble growth cycle.

Effect of Solid Walls on Bubble Growth

Figure (6) shows the computed effect of the proximity of the solid wall on bubble growth. Two cases are considered. In case "A" the wall is 6cm from the centreline of the orifice whilst in case "B" this distance is 2cm. Both computations were performed for the conditions R_h = 0.16cm, V_c = 2250cm^3, G = 16.7cm^3 per second.

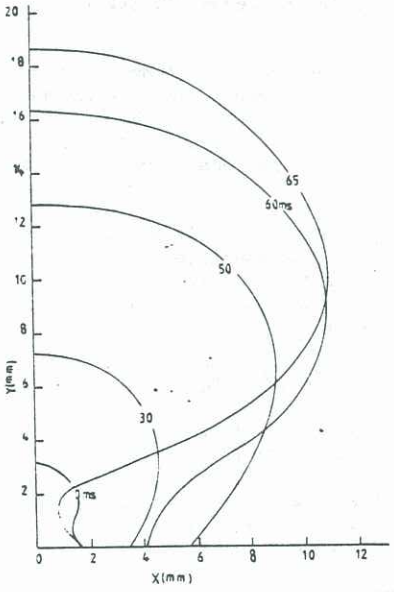

Figure 4 - Computed bubble shapes for the experimental conditions of Kupferberg and Jameson (1969).

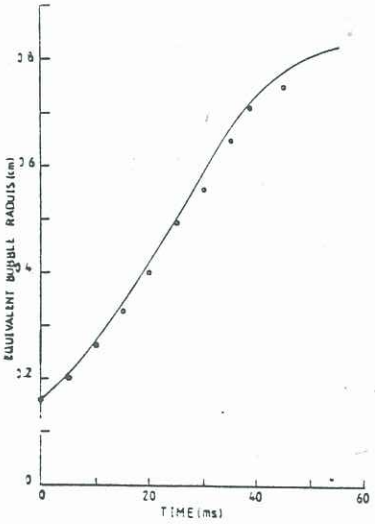

Figure 5 - Comparison between model and experimental data of Kupferberg and Jameson (1969).

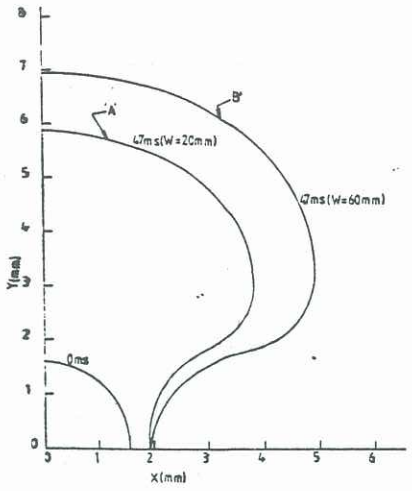

Figure 6 - Computed effect of solid wall on bubble growth

The results clearly show that the effect of the solid wall on bubble growth is significant. The bubble size at comparable growth times is smaller for the case where the wall is closer to the orifice. This is the first time that the effect of the wall on bubble growth has been predicted theoretically.

5 CONCLUSION

A model based on a modified MAC method has been developed to describe the process of bubbling at a submerged orifice. The agreement between the model and the experiments is good and the model shows that bubble growth is non-spherical abd that bubble detachment arises as a natural consequence of the dynamics of the system.

Computations based on the model show that bubble growth is significantly affected by the presence of solid walls which act to limit the extent of the liquid flow field. All previously proposed models of bubble formation assume that the liquid is of infinite extents and therefore cannot predict this effect of solid walls on bubble growth. The present model therefore represents a significant improvement over previous models and should prove useful in the analysis of the 'shallow-pool' or imperfect bubbling regimes where previous models have not been applicable.

6 REFERENCES

Chan, R.K-C.and Street, R.L. (1969) J.Computational Physics, 6, p. 68

Davidson, J.R. and Schuler, B.O.G. (1960) Trans.Inst. Chem.Engrs. 38 p. 335

Harlow, F.H. and Welch, J.E. (1965) Phys.Fluids, 8 p. 2182

Kupferberg, A, and Jameson G.T. (1969) Trans.Inst.Chem. Engrs. 47 p.241

Marmur, A. and Rubin, E. (1976) Chem.Engng.Sci., 31 p. 453

McCann, D.J. and Prince, R.G.H., (1969) Chem.Engn.Sci. 24, p.801

McCann, D.J. and Prince, R.G.H., (1971) Chem.Engng.Sci. 26, p.1505

Pinczewski, W.V. (1981) Chem.Engng.Sci. 36, p. 405